Polymer Degradation and Stability (2013). 98(6), 1188-1195.
DOI: http://dx.doi.org/10.1016/j.polymdegradstab.2013.03.018

Thermal stability and degradation kinetics of feedstocks for powder injection moulding e A new way to determine optimal solid loading?

J. Hidalgo [a,*], A. Jiménez-Morales [a], J.M. Torralba [a,b]

[a] *Materials Science Department at Carlos III University of Madrid, Avd. Universidad 30, 28911 Leganés, Spain*
[b] *IMDEA Materials Institute, Getafe, Spain*
[*] Corresponding author. Tel.: +34 916249482. *E-mail address:* jhidalgo@ing.uc3m.es (J. Hidalgo).

Abstract: Degradation kinetics and the thermal stability of zircon powder injection moulding feedstocks (PIM) based on cellulose acetate butyrate (CAB) and polyethylene glycol (PEG) binders were investigated using simultaneous thermogravimetric analysis (STA). The initial decomposition temperature (IDT) and the integral procedure decomposition temperature (IPDT) were used to analyse the thermal stability of the binder system as a function of the solid loading content. The degradation kinetics was studied, and the degradation activation energy was assessed for varying zircon powder contents using isoconversional methods. All the methodologies revealed changes in the thermal degradation behaviours of the feed-stocks for solid loadings that were previously determined to correspond to optimal solid loadings using other experimental procedures. These results may promote the proposal of thermodynamic degradation studies of feedstocks as an alternative or complementary technique to determine optimal solid loading contents in powder injection moulding (PIM). The studies in this paper also examined PIM process operation temperatures for zircon feedstocks.

Keywords: Powder injection moulding, Zircon, Cellulose acetate butyrate, Polyethylene glycol, Thermal degradation.

1. Introduction

Powder injection moulding (PIM) is one of the main manufacturing processes used to produce small parts with complex geometries, thin walls and in large production batches [1,2]. This technology is applied to a wide variety of ceramics, metallics and combinations thereof [3]. The process consists of mixing a fine powder material with different polymer-like compounds, the so-called binder system. The binder system provides sufficient fluidity to the newly created feedstock to allow mould filling during injection and easy removal during the subsequent debinding process. The binder system must be added in such quantities so as to optimise the process conditions and time required. The volume occupied by the binder decreases during debinding, and the density of the powder particles increases during sintering to achieve the final part properties. Shrinkage occurs as consequence of sintering. To minimise shrinkage and increase part tolerances, the maximum powder volume fraction is desired. This powder particle fraction is limited by rheological factors and by technical considerations during debinding. The particle volume fraction ranges from 50 vol.% to approximately 70 vol.%, depending on the powder and binder characteristics. At present, the optimal solid loading is determined by rheologic measurements and the final part properties.

Currently, there are various sophisticated methods of eliminating polymeric components of the feedstock, but debinding normally requires two consecutive stages. First, one of the binder components is removed by a physical solvent process that creates interconnected channels to facilitate the removal of volatiles during a second thermal debinding stage. This procedure not only prevents defects by relieving the internal pressure from any trapped volatiles but also allows a more rapid elimination of volatiles than a single thermal step process. Powder particles constitute a barrier for both polymer chains that are removed by solvent and volatile products resulting from thermal degradation, which limits the effectiveness of the debinding. Moreover, during thermal debinding, atmospheric and temperature conditions are important considerations. For typical polymer decomposition temperatures, the probability of material contamination with elements such as carbon or oxygen becomes especially important for metallic materials. Therefore, a thermal debinding process preferably uses an inert atmosphere whenever possible, although oxygen is more effective for organic component degradation.

Polymer decomposition mechanisms within the feedstock are very complex. The decomposition of a single binder component by itself is complex, as in PEG decomposition in an inert gas. Polyethylene glycol (Fig. 1b) is a polyether compound formed by the polymerisation of ethylene oxide monomers with conforming

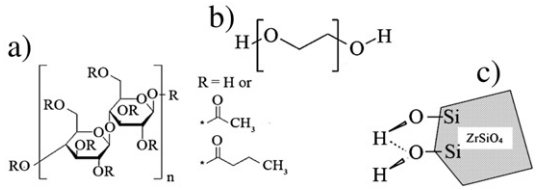

Fig. 1. The chemical structures of the different feedstock components: a) the basic cellulose acetate butyrate monomer and possible substitution groups; b) poly(-ethylene) glycol monomer and end chain hydroxyl groups; and c) a representation of the hydroxyl groups on the zirconium silicate particle surface.

linear chains. There is extensive literature describing the thermal degradation of PEG in terms of the decomposition of volatiles or the pyrolysis of by-products studied with chromatography, infrared spectroscopy or mass spectroscopy [4,5]. The products obtained during PEG pyrolysis include various formaldehydes, acetaldehydes, ethylene glycol, ethylene oxide, water, low-carbon alkenes, carbon monoxide and dioxide and traces of other low molecular weight hydroxyl, carboxyl, carbonyl and ethereal compounds. The decomposition of CAB, an ester of cellulose that includes not only its main constituent monomers (beta-D-glucose chains) but also variable substitution of butyryl, acetyl and hydroxyl side groups, results in even more complex products (Fig. 1a). Cellulose pyrolysis has been studied for more than six decades. Even so, the molecular-level processes underlying the pyrolysis reactions remain poorly understood. Gongwer et al. detected carbon monoxide, carbon dioxide, methyl acetate and methyl butyrate among the volatile fractions derived from CAB pyrolysis with certain amounts of ketenes and ethyl ketenes, butyric and acetic acid [6]. That study showed the complexity of the products that presumably result from feedstock degradation. On the one hand, the findings indicate the probable influence of the different interactions among constituents on the global decomposition behaviour. Zirconium silicate surface and hydroxyl groups (Fig. 1c) most likely interact with side or end groups present in the CAB and PEG chains. On the other hand, degradation compounds from the less thermally stable polymers may also affect the onset temperature of the most thermally stable polymer. Furthermore, particles act as a barrier to the removal of volatiles and, thus, affect the degradation rate.

In this work, simultaneous calorimetry and thermogravimetric analyses were performed to study the thermal decomposition of zirconium silicate feedstocks composed of cellulose acetate butyrate (CAB) and polyethylene glycol (PEG) binders in an inert nitrogen atmosphere. Binder and feedstock temperature stability and decomposition kinetics were investigated using integral procedure decomposition temperature (IPDT) and isoconversional methodologies, respectively. Several isoconversional methods were used, and their convenience is discussed. The FTIR technique was used to investigate possible interactions between feedstock components.

Several zirconium silicate feedstocks consisting of mixtures with different proportions of constituents were investigated; these variations allowed the effect of the effective powder surface on the chemisorption of CAB and PEG molecules and the channel volume used to remove volatiles to be elucidated. The degradation of the binder system was studied to evaluate the extent of the influence that particles exert on the decomposition of CAB and PEG. The results reveal changes in the thermal degradation behaviour with solid loading. Based on the findings, a method to determine the optimum solid loading conditions using thermogravimetric tools is proposed and discussed.

2. Experimental

Zirconium silicate powders were supplied by GUZMÁN GLOBAL S.L. (Nules, Spain) and exhibit an irregular, edged morphology. A Malvern 2000 laser scattering device was used to measure the particle distribution parameter. The particle size parameters (D_{50} and D_{90}) are 1604 and 465 μm, respectively. The powders have a specific surface area of 5.0363 m^2/g, as measured with a Micrometrics Gemini VII BET measurement device.

A binder system based on PEG and CAB was selected. These binders have been demonstrated to be effective for zircon PIM and provide improved properties when compared to other binder systems [7]. However, there are no published comprehensive studies on their thermal degradation. The binders consist of two types of CAB: CAB381-0.1 and CAB551-0.01. Each of these binders has different percentages of butyryl, acetyl and hydroxyl groups blended with two types of PEG with different average molecular weights. The composition of the binder system and the characteristics of the components are shown in Table 1.

A Rheomix 600 Haake rheometer coupled with a Haake Rheocord 252p module was used for the mixing experiments. Different feedstock compositions, ranging from 0 vol.% zircon powder (single binder) to 52.5 vol.% (minimum solid loading tested) to 65 vol.%, were investigated in 2.5 vol.% increments. A temperature of 150 °C was used for all the batches, and the mixing chamber was filled with feedstock to 72% of the total volume (the chamber volume is 69 cm^3). A rotor speed of 50 rpm was employed to mix the feedstock and the binder for 60 min to ensure complete homogenisation. In addition, a batch was produced by dissolving all of the binder components in an ethylene acetate solvent and placing it in a vacuum at 120 °C for 8 h to ensure maximum homogenisation of the polymer components.

A Perkin Elmer STA 6000 device was used to thermodynamically evaluate the decomposition of the binder and the feedstock. This device allows the simultaneous acquisition of the thermogravimetric TGA curves and the DTA/DSC curves. The examined temperature range was from 50 °C to 650 °C. Calcium oxalate was employed for thermogravimetric calibration, whereas elemental indium (99.999% pure) was used for heat and temperature calibration. An inert nitrogen atmosphere was employed with a flow rate of 40 ml/min. Feedstock pellets of approximately the same morphology and weight were used for the analysis. The net weight of the binder in the feedstock was constant for all experiments, with a minimum of 5 mg for all cases. For a thorough evaluation of the decomposition kinetics, four heating rates were evaluated: 10 °C/min, 15 °C/min, 20 °C/min and 25 °C/min.

A Philips XL 30 scanning electron microscope (SEM) and an Olympus GX71 light optical microscope (LM) with a polarised filter were used to determine the homogenisation. Fourier transform infrared spectroscopy (FTIR) measurements were recorded using a Perkin Elmer Spectrum GX device.

3. Results

3.1. Thermal degradation of binder in N_2

Fig. 2 presents typical differential scanning calorimetry curves (DSC), thermogravimetry (TG) curves (or thermograms) and the derivative of the TG curves (DTG) for feedstocks in a nitrogen

Table 1
Composition of the binder material.

	CAB381-0.1	CAB551-0.01	PEG20k	PEG4k
Vol.%	10	30	58	2
T_{MELT} [°C]	155–165	127–142	63–66	58–61
T_{GLASS} [°C]	123	85	<0	<0
M_W	20,000	16,000	20,000	4000
Supplier	Eastman	Eastman	Aldrich	Aldrich

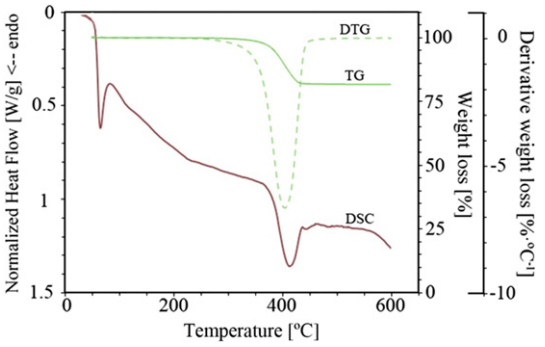

Fig. 2. Typical simultaneous thermal analysis of the DSC, TG and DTG curves of the studied feedstocks. In this case, the curves correspond to a 52.5 vol.% feedstock subjected to a heating rate of 20 °C/min.

atmosphere. The characteristic PEG melting peak can be observed between 50 °C and 70 °C in the DSC curve. The degradation temperature interval occurs between 350 °C and 440 °C and represents a single endothermic step.

The resulting TGA thermograms for different feedstock solid loadings at a heating rate of 20 °C/min are presented in Fig. 3. The theoretical values of the maximum weight loss possible for these systems are represented by straight, dashed lines. None of the tests achieved complete thermal degradation of the polymer components, which suggests that for a nitrogen atmosphere, there is a residual portion of the binder component that does not degrade completely under these conditions up to 600 °C. Thus, this residue corresponds to incomplete CAB degradation.

The deviation from the theoretical value is considerably higher for feedstocks with lower solid loading content and diminishes as the solid loading increases. As the solid loading content increases, the polymer weight that must be eliminated within the same time frame decreases; as a result, the deviation from the theoretical value will presumably decrease. Nevertheless, the deviations of the 52.5 vol.% and 55 vol.% feedstocks are high compared to those of the other feedstocks at higher solid loadings. A possible explanation could be a decrease in the organic compound molecular weight caused by mechanical scission of the chains. As the solid loading increases, the particles become arranged in a closer packing configuration, which increases the probability of particle contact despite the existence of a separating polymer gap. This arrangement increases the shear forces that support the binder components. Therefore, mechanical scission of the polymer chain may occur. As the polymer molecular weight decreases, the effectiveness of the thermal degradation in terms of the remaining residue increases.

Nevertheless, the thermogram slope decreases as the solid loading increases. To some extent, this trend is contrary to the theoretical reduction in the binder molecular weight caused by increasing shear forces. The slope, which represents the weight loss ratio for different temperature increments, is an indicator of how the binder components are decomposed and removed from the system. The slope change has several interpretations, and its meaning remains controversial in high charged polymer systems. For high solid loading content, this trend may reveal increasing difficulty in removing decomposed volatiles because of the formation of a char layer or particle impediment as the solid loading increases for PIM feedstock. This issue has been extensively studied for systems in which the solid content is relatively low (up to 50 vol.%), especially in epoxy resins that are thermally stabilised with fillers [8,9]. In such cases, many works attribute this decrease in the slope to the formation of a char layer, which contributes to the polymer thermal stability. In PIM systems, this behaviour is explained by the increasing packing of the powder particles because the solid load impedes the formation of evacuating channels or reduces their capacity by decreasing their cross section; these effects are enhanced by the formation of a char layer around the particles.

As can be observed from Fig. 2, for all of the feedstocks DTG curves, the decomposition of binder components in nitrogen, although it is a complex multi-component system, occurs in a single step via a dominant decomposition reaction or via concurrent decomposition reactions that occur within the same temperature range. This finding is in contrast to the two well-defined CAB and PEG degradation DTG peaks recorded for the binder system alone (Fig. 4). The DTG peaks of each binder component without zircon powders (both separately and after mixing) are shown in Fig. 4. The temperature for the maximum weight loss rate differs greatly between the CAB and PEG raw components. A small deviation is observed in the onset temperature, as well as a widening of the CAB degradation peak in the DTG curves for the binder system; these trends are observed when the binder components were mixed by mechanical and solvent methods, which may reveal a certain interaction between the PEG and CAB components. There is a single peak in the DTG curve of the feedstock, which shows that a certain type of interaction between the powders and the binder component may be occurring (i.e., chemisorptions of the OH or C=O carbonyl groups with zircon OH present on the particle surfaces). The degree of compatibility between CAB and PEG is directly related to the solubility or miscibility of these components, which could be such that, even after mixing by dissolution in a common solvent to promote maximum polymer chain entanglement, some rejection may occur between the components and lead to the formation of different phases. This effect is shown in Fig. 5 where three phases are observed in the binder system without filler: a) a typical PEG micelle, b) an amorphous CAB region and c) a mixture of both CAB and PEG in a fibre structure.

If there is an interaction between the binder components and the particle surfaces, the points at which these interactions occur may act as anchor points to prevent component segregation and promote

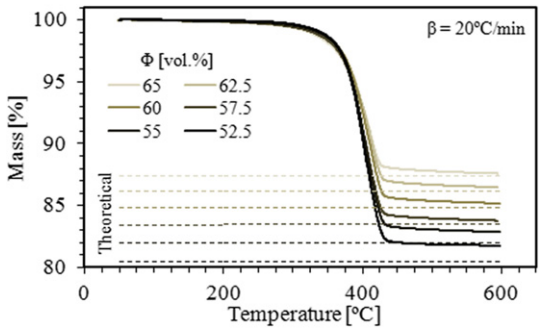

Fig. 3. TGA weight loss results for different solid loadings.

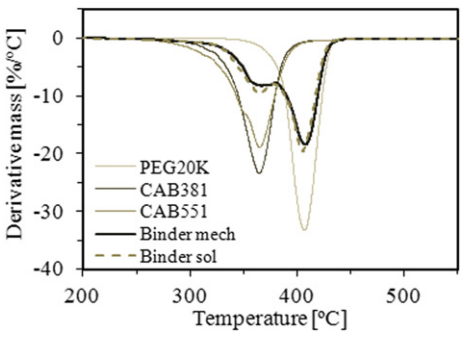

Fig. 4. DTG curves of the mechanically mixed binder system (Binder mech), the ethylene acetate solvent mixture (Binder sol) and their individual components.

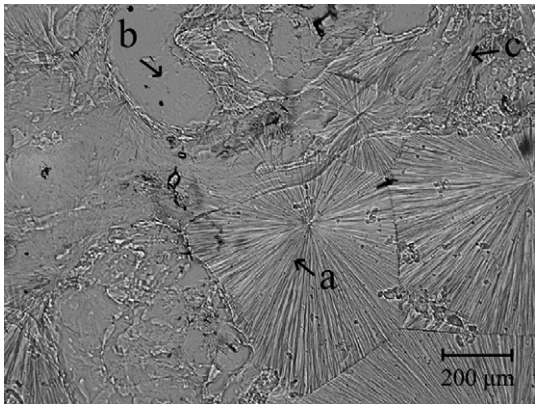

Fig. 5. Polarised light optical microscopy image of the binder system: a) a typical PEG micelle; b) a region of pure CAB; and c) a region with a phase presumed to be a mixture of CAB and PEG.

the formation of smaller single component phases. This process is observed in Fig. 6, which contains a scanning electron microscopy (SEM) image of the zircon feedstock. The zircon particles are homogeneously embedded in a homogenously mixed binder system. The CAB fibres interconnect the particles, and PEG surrounds both the CAB and zircon particles. This arrangement explains why the CAB and PEG degradation DTG peaks merge into a single peak.

To evaluate any possible interactions between the powder and binder components, FTIR experiments were performed for individual binder components, for the binder system itself and for the feedstock containing zircon powder. The resulting FTIR absorption spectra for the wave number range from 1600 to 4000 cm^{-1} are presented in Fig. 7. The baselines were subtracted, and the curves were normalised to the maximum peak value. Additionally, there is a slight red shift (approximately 8 cm^{-1}) of the characteristic CAB peak (1757.6 cm^{-1}) in the case of the feedstock but not in the binder system. This peak is related to the carbonyl group present in acetyl and butyryl substituents in CAB. There is also a slight red shift (approximately 10 cm^{-1}) of the characteristic PEG peak (2884.8 cm^{-1}) that is only observed in the feedstock. These peak displacements, along with the LOM and SEM images, are sufficient to dismiss possible experimental resolution error (1 cm^{-1}) and are evidence of certain interactions between the powder and binder components that explain the behaviour of the DTG curves. The specific nature of these interactions is not discussed in this work.

3.2. Thermal stability studies

The initial decomposition temperature (IDT) and the integral procedure decomposition temperature (IPDT) were used to analyse

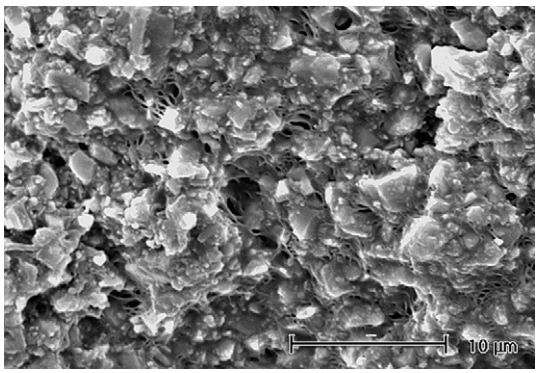

Fig. 6. Scanning electron microscopy (SEM) image of the zircon feedstock. The zircon particles are homogeneously embedded in a homogenously mixed binder system.

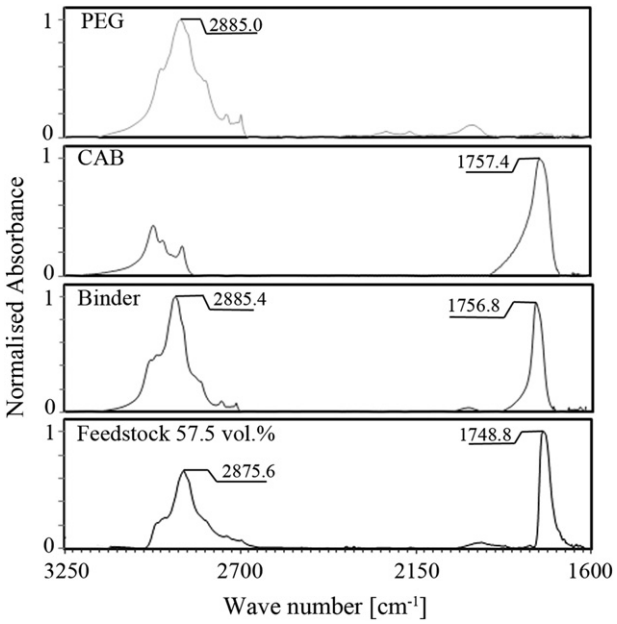

Fig. 7. Fourier transform infrared (FTIR) spectra. From top to bottom: PEG20k, CAB381, binder system and 57.5 vol.% feedstock. The curves were smoothed, base-line subtracted and normalised, but the peak values were determined from the original curves to avoid correction distortions.

the thermal stability of the binder system as a function of the solid loading content. The IDT indicates the apparent thermal stability of binder system with regard to the maximum feedstock processing rate and moulding temperatures. The IDT is determined by the onset weight loss in the TGA curves of the different feedstocks. Table 2 presents the values of the degradation onset temperature (IDT), maximum thermogram derivative peak (T_{max}) corresponding to the temperature at the maximum degradation rate, degradation end temperature (T_{end}) and the wide thermogram derivative peak (ΔTpeak). The IDT and T_{end} values decrease when the solid loading increases; additionally, the peak widens, and T_{max} rises. The decrease in the onset and ending temperatures may indicate an incremental decrease in the binder molecular weights caused by the shear forces exerted by the powder particles on the binder components as the solid loading increases. However, the T_{max} increment suggests the weight loss decreased as the proportion of the zircon particles increases by an impediment of zircon particles.

The IPDT determined from the residual weight fraction in the TGA is a reproducible datum that can be consistently determined for diverse materials and represents both a truly comprehensive index of intrinsic thermal stability and a real temperature that has practical significance. The method for calculating the IPDT is proposed by Doyle [8,10] and converts the area under the TGA curve into a value that approximately represents the characteristic end-of-volatilisation temperature, T_{a^*} (Eq. (1)):

Table 2
Thermal parameters deduced from the TG and DTG curves for different solid loadings.

Φ [vol.%]	IDT [°C]	T_{max} [°C]	T_{end} [°C]	ΔTpeak [°C]	IPDT [°C]
52.5	358.5	403.3	437.9	79.4	3846.8
55	359.0	404.4	437.8	78.8	4126.2
57.5	356.4	407.5	436.3	79.9	4398.4
60	356.3	411.2	436.9	80.6	4863.8
62.5	353.2	411.5	435.9	82.7	5376.3
65	351.4	410.9	433.6	82.2	5962.5

$$T_{a^*}[^\circ\mathrm{C}] = A^* \cdot \left(T_\mathrm{f} - T_\mathrm{i}\right) + T_\mathrm{i}, \quad (1)$$

where A^* is the area under the TGA curve within the evaluated temperature range (defined by initial temperature T_i and the final temperature T_f) and normalised with respect to both the residual weight and temperature. However, the IPDT takes into account the amount of refractory or non-volatile residues at T_f by means of the coefficient K^*. Therefore, the method to calculate the IPDT is described in Eq. (2):

$$\mathrm{IPDT}[^\circ\mathrm{C}] = A^* \cdot K^* \cdot \left(T_\mathrm{f} - T_\mathrm{i}\right) + T_\mathrm{i}. \quad (2)$$

A representation of the areas S_1, S_2 and S_3 used to calculate A^* $[A^* = (S_1 + S_2)/(S_1 + S_2 + S_3)]$ and K^* $[K^* = (S_1 + S_2)/S_1]$ is shown in Fig. 8. In these cases, the IPDT represents the inherent thermal stability of the binder system and describes the entire binder degradation process in terms of the decomposition and vaporisation of the different volatiles taking into account differences in the solid loading percentages. The higher the IPDT is, the more thermally stable the feedstock is. Thus, the binder components will resist higher temperatures until complete volatilisation occurs.

IPDT values for different solid loading feedstocks and heating rates are presented in Fig. 9. The value of the IPDT increases as the solid loading increases. Increasing the solid loading reduces the volatile fraction and the fraction of char formation that would reduce the release of volatiles. Good thermal stability, heat-resistant properties and the high content of zirconium silicate powder particles reduce both the thermal degradation rate of the organic component of the feedstocks and the thermal stability. Two linear tendencies are observed in the plotted data. The first occurs below 57.5 vol.% solid loading and has a smoother slope than the second, which occurs for values greater than 57.5 vol.%. This change in the slope coincides with the optimum solid loading values determined for powder injection moulding in previous works with zirconium silicate feedstocks, as determined using rheological methods [11].

3.3. Thermal degradation kinetics in nitrogen atmosphere

Non-isothermal isoconversional methods are chosen to study degradation kinetics of the selected PIM feedstocks. The main reason to select these methodologies instead of isothermal procedures is due to simplicity and to take in advance the conventional non-isothermal TGA curves that are employed in some steps optimisation in PIM processes. Although non-isothermal approaches have several limitations in their use to ascertain kinetics parameters, they are frequently used to study the kinetics of charged polymers [12,13]. These methods are based on studying the degree of conversion with respect to temperature at different heating rates. As an example, Fig. 10 represents the typical conversion curves for zircon feedstocks at different heating rates; in this particular case, the loading is 60 vol.% feedstock. The degree of conversion for a certain temperature α is defined as the ratio of the actual weight loss $m(T)$ to the total weight loss, as expressed in Eq. (3):

$$\alpha(T) = \frac{m_0 - m(T)}{m_0 - m_\infty}. \quad (3)$$

The variables m_0 and m_∞ correspond to the initial and final masses, respectively. Unlike classical model-fitting methods, isoconversional methods do not assume a kinetic model $f(\alpha)$ to calculate the activation energy of a reaction. Instead, the apparent activation energy is calculated directly from the TGA curves. Consequently, the rate of degradation, $\mathrm{d}\alpha/\mathrm{d}t$, is assumed to depend on the temperature and weight of the sample. The main advantage of eliminating the necessity of a kinetic model, which for complicate reactions could result a complex task, is clouded by the influence of the sample mass and size in the apparent kinetics parameters calculated. Furthermore these parameters could be influenced by the thermal lag across the specimen [14].

In literature a wide variety of non-isothermal models could be found. The lack of agreement among kinetic parameters calculated from the same set of experimental data using different methods of mathematical analysis is disturbing. In this work FWO and KAS integral methods are selected to estimate apparent activation energy values. They are based in the integral of the following expression (Eq. 4):

$$\frac{\mathrm{d}\alpha}{f(\alpha)} = \left(\frac{k_0 \cdot \exp(-E_a/R \cdot T)}{\beta}\right) \cdot \mathrm{d}T, \quad (4)$$

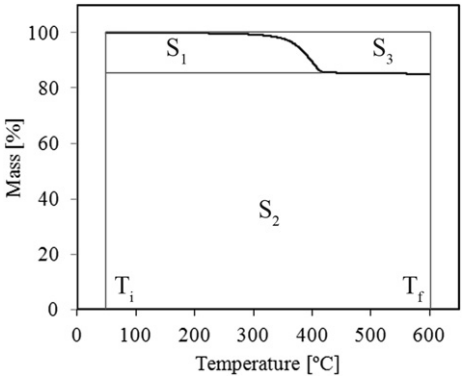

Fig. 8. Schematic representation of S_1, S_2 and S_3 for the IPDT (60 vol.%, 10 °C/min and N_2).

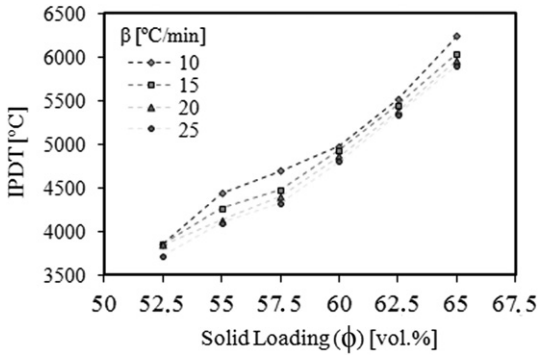

Fig. 9. IPDT values for different solid loadings and heating rates.

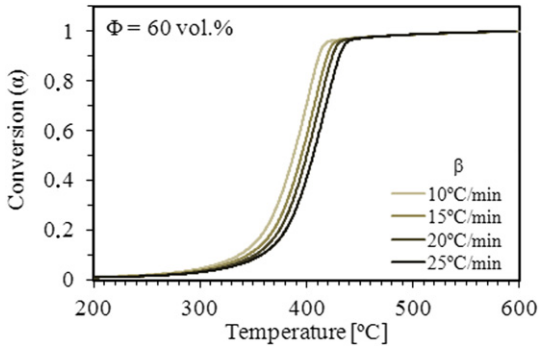

Fig. 10. Typical conversion curves for zircon feedstocks at different heating rates (60 vol.% solid loading).

where k_0 represents the pre-exponential factor, or frequency factor; E_a is the apparent activation energy; R is the gas constant; T is the absolute temperature; and β is the heating rate (dT/dt).

The FWO [15,16] method is based on the principle that a reaction rate at a constant conversion is only a function of temperature. Using Doyle's approximation [17] of the temperature integral $p(E_a/R{\cdot}T)$ and applying logarithms, the following expression is produced (Eq. (5)):

$$\log(\beta_i) = \log\left[\frac{k_0 \cdot E_a}{R \cdot g(\alpha)}\right] - 2.315 - 0.4567 \cdot \left(\frac{E_a}{R \cdot T_{\alpha i}}\right), \quad (5)$$

where $g(\alpha)$ represents the integral of $d\alpha/f(\alpha)$. Considering a constant conversion, the representation of $\log \beta$ vs. $1/T$ should be a straight line with a slope defined as $d(\log \beta)/d(1/T) = -0.4567(E_a/R{\cdot}T)$. Therefore, the activation energy may be calculated from Eq. (6) as follows:

$$E_a = -\text{slope} \cdot \frac{R}{0.457}. \quad (6)$$

The Kissinger–Akahira–Sunose method (KAS method) [18,19] (Eq. (7)) is based on the Coats–Redfern [20] approximation of the temperature integral $p(E_a/R{\cdot}T)$. The resulting relationships are expressed as:

$$\ln\left(\frac{\beta_i}{T_{\alpha i}^2}\right) = \ln\left(\frac{k_0 \cdot R}{E_a \cdot g(\alpha)}\right) - \frac{E_a}{R \cdot T_{\alpha i}}. \quad (7)$$

Thus, the plot of $\ln(\beta/T^2)$ vs. $1/T^2$ for constant values of α and αi should be a straight line with a slope that can be used to calculate the apparent activation energy (Eq. (8)):

$$E_a = -\text{slope} \cdot R. \quad (8)$$

Some of the main shortcomings of both methods are using an approximation of the temperature integral and the selection of the integral limits, but the validity of the calculated apparent activation energies is assumed good enough for the general propose of this work.

Fig. 11 shows the typical isoconversional curves of the FWO and KAS methods from which the apparent activation energy can be obtained. Both methodologies present a relatively good linear correlation with the experimental results, but the FWO method is more precise according to correlation coefficient. Table 3 presents some activation energy results and the corresponding correlation coefficient R^2 for each method. The KAS and FWO methods allow the calculation of the activation energy at different conversion values.

Fig. 12 shows the dependence on conversion of the apparent activation energy values, as assessed by the FWO and the KAS methods. Differences in the calculated values of the activation energies evidence the limitations of using non-isothermal approaches. Through α, the feedstocks seem to have an important influence on E_a that is independent of solid loading. Increasing dependence of the activation energy on the conversion is quite typical of polymer degradation [21]. This behaviour is considered to be an indicator of a complex reaction [22]. For the majority of the curve, E_a increases as the values of α increase up to a value at which E_a either stabilises or begins to decrease; this behaviour gives the curve a certain convexity. Vyazovkin and Lesnikovich [23,24] noted that in non-isothermal experiments, patterns in the shape of the curve dependence of the apparent value of E_a on α could provide insight into the type of complex process taking place. An increasing dependence of E_a on α characterises concurrent, competitive reactions, whereas convexity indicates a change in the rate-determining step.

Table 3
Various activation energies calculated by different methods: FWO, KAS and Kissinger (considering both the DSC peaks and the DTG peaks).

60 vol.%	FWO		KAS	
A	E_a [kJ/mol]	R^2	E_a [kJ/mol]	R^2
0.3	165.7	0.993	252.5	0.983
0.4	172.9	0.993	263.8	0.983
0.5	179.1	0.987	272.6	0.971
0.6	186.3	0.993	285.1	0.983
0.7	186.9	0.991	285.5	0.980
Average	178.2		271.9	

The concurrent competitive reactions could be molecular degradation reactions of both CAB and PEG. The subsequent plateau at high conversion values may indicate the end of a reaction or the creation of open pathways that facilitate the removal of volatiles as the binder decomposes. Unfortunately non-isothermal methods without other supporting information have generally a no-mechanistic value, but at least in this case could serve as a first rough approach to support the general analysis in combination with other methodologies presented.

Fig. 13 represents the activation energies for a constant conversion of 0.4 for different feedstock solid loadings. A minimum activation energy is observed at 60 vol.%, which coincides with a minimum in the activation energy calculated by Hidalgo [11] using rheological methods for the same feedstocks.

This phenomenon may be explained by opposing effects. First, a reduction in the molecular weight of the polymer compound caused by shear forces as the solid loading increases reduces the activation energy. Simultaneously, a portion of the effective particle surface presumably interacts with the polymer compound and reduces the apparent activation energy of degradation. The opposite effect, an increase in the apparent activation energy, would occur as a

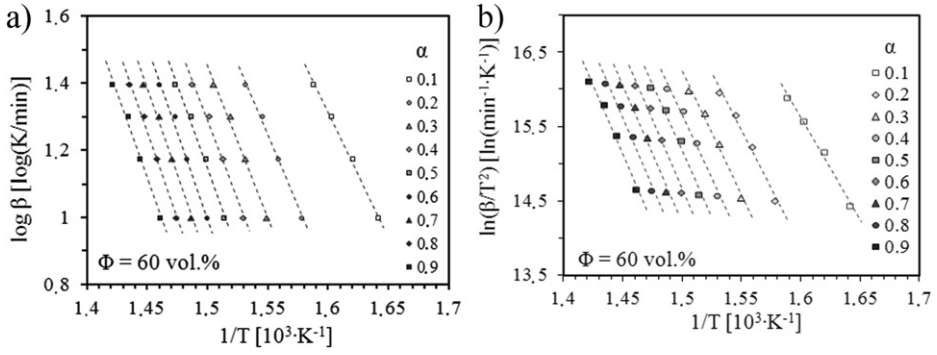

Fig. 11. Isoconversional plots used to calculate the activation energy at the listed conversion α values by a) the FWO method and b) the KAS method for 60 vol.% zircon feedstock.

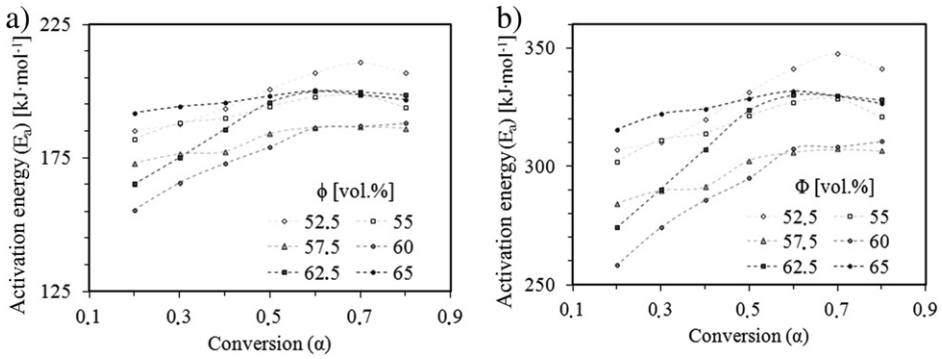

Fig. 12. Dependence of the apparent activation energy on the conversion assessed using a) the FWO and b) the KAS methods.

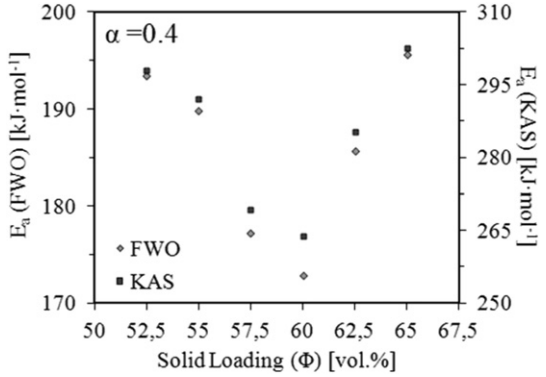

Fig. 13. The activation energy dependence on the conversion.

consequence of particle packing as the solid loading increases, reducing the diameters of the volatiles-removal channels that may have been enhanced by the formation of a protective layer of char around the particles. All of these effects combine to minimise the apparent activation energy of degradation, reaffirming 60 vol.% as the optimum solid loading value with respect to both rheological concerns and thermal degradation of the binder. The direct relationship between the apparent activation energies, with respect to both rheological and thermal degradation concerns, is not clear. There are analogies in the possible explanations of the mechanisms that affect these factors, such as the change of the particle packing and the effective interaction surface between the organic compounds and the particles. Nevertheless, studying the thermal degradation by calculating activation energies for different solid loading conditions emerges as an alternative to the traditional rheological studies used to assess optimal solid loading in PIM feedstocks.

4. Conclusions

Thermal analyses via DSC and TG experiments in a nitrogen atmosphere were performed for different solid loading zircon feedstocks composed of CAB and PEG. Binder components apparently thermally degrade by endothermic concurrent reactions in a single step between 350 °C and 430 °C. A possible interaction between the zircon particles and the binder components was revealed by this single peak and the infrared FTIR analysis. Thermal stability studies using the IPDT factor reveal a linear slope in the feedstock thermal stability as the solid loading increases. A change in the linear slope occurs at approximately 60 vol.% solid loading. This change coincides with the optimal solid loading calculated in previous studies using rheological methods. The kinetics of the thermal degradation of the binder components in terms of calculation apparent activations energies was also studied using the FWO and KAS methods. Variations in the apparent activation energies calculated using these methods suggest the occurrence of complex, concurrent and competitive reactions. A representation of the apparent activation energy at a constant conversion for different solid loadings shows that the activation energy is minimised at 60 vol.%. This value coincides with a minimum in the activation energy calculated using rheological methods in previous studies. All of these results emphasise the potential for using thermocalorimetric analysis instead of, or as a complement to, conventional rheological studies to determine the optimal solid loading of PIM feedstocks.

Acknowledgements

The authors wish to acknowledge M. Crespo for her generously provided comments and discussion of the results. The authors also wish to thank GUZMÁN GLOBAL S.L. and MIMTECH ALFA for their collaboration on the ECOPIM project (ref. IPT-2011-0931-20000) that was funded by the Spanish Ministry of the Economy and Competitiveness. Furthermore, the authors would like to acknowledge the strong support from the ESTRUMAT projects (ref. S2009/MAT-1585), which were funded by the CAM-Consejería Educación Dir. Gral. Universidades e Investigación, and from the COMETAS project (ref. MAT2009/14448-C02-02), which was funded by the Spanish Ministry of the Economy and Competitiveness.

References

[1] German RM, Bose A. Injection molding of metals and ceramics. Metal Powders Industry Federation; 1997.
[2] German R. Metal powder injection molding (MIM): key trends and markets. In: Heaney D, editor. Handbook of metal injection molding. Woodhead Publishing Limited; 2012.
[3] Petzoldt F. Current status and future perspectives of the MIM technology. Ceramic Forum International 2012;89:E11–5.
[4] Voorhees KJ, Baugh SF, Stevenson DN. An investigation of the thermal-degradation of poly(ethylene glycol). Journal of Analytical and Applied Pyrolysis 1994;30:47–57.
[5] Arisawa H, Brill TB. Flash pyrolysis of polyethyleneglycol. 1. Chemometric resolution of FTIR spectra of the volatile products at 370-550 degrees C. Combustion and Flame 1997;109:87–104.
[6] Gongwer PE, Arisawa H, Brill TB. Kinetics and products from flash pyrolysis of cellulose acetate butyrate (CAB) at 460-600 degrees C. Combustion and Flame 1997;109:370–81.
[7] Bernardo E, Hidalgo J, Jimenez-Morales A, Torralba JM. Feedstock development for powder injection moulding of zirconium silicate. Powder Injection Moulding International 2012;6:4.
[8] Jin F-L, Park S-J. Thermal properties of epoxy resin/filler hybrid composites. Polymer Degradation and Stability 2012;97:2148–53.
[9] Tarrio-Saaavedra J, Lopez-Beceiro J, Naya S, Artiaga R. Effect of silica content on thermal stability of fumed silica/epoxy composites. Polymer Degradation and Stability 2008;93:2133–7.
[10] Doyle CD. Estimating thermal stability of experimental polymers by empirical thermogravimetric analysis. Analytical Chemistry 1961;33:77.

[11] Hidalgo J, Jimenez-Morales A, Torralba JM. Torque rheology of zircon feedstocks for powder injection moulding. Journal of the European Ceramic Society 2012;32:4063−72.
[12] Jankovic B, Marinovic-Cincovic M, Jovanovic V, Samarzija-Jovanovic S, Markovic G. The comparative kinetic analysis of non-isothermal degradation process of acrylonitrile-butadiene/ethylene-propylene-diene rubber blends reinforced with carbon black/silica fillers. Part II. Thermochimica Acta 2012;543:304−12.
[13] Macan J, Brnardic I, Orlic S, Ivankovic H, Ivankovic M. Thermal degradation of epoxy-silica organic-inorganic hybrid materials. Polymer Degradation and Stability 2006;91:122−7.
[14] Holland BJ, Hay JN. The value and limitations of non-isothermal kinetics in the study of polymer degradation. Thermochimica Acta 2002;388:253−73.
[15] Flynn JH, Wall LA. A quick direct method for determination of activation energy from thermogravimetric data. Journal of Polymer Science Part B-Polymer Letters 1966;4:323.
[16] Ozawa T. A new method of analyzing thermogravimetric data. Bulletin of the Chemical Society of Japan 1965;38:1881.
[17] Doyle CD. Series approximations to equation of thermogravimetric data. Nature 1965;207:290.
[18] Kissinger HE. Reaction kinetics in differential thermal analysis. Analytical Chemistry 1957;29:1702−6.
[19] Akahira T, Sunose T. Joint convention of four electrical institutes. Chiba: Chiba Institute of Technology; 197122−31.
[20] Coats AW, Redfern JP. Kinetic parameters from thermogravimetric data. Nature 1964;201:68.
[21] Vyazovkin S, Sbirrazzuoli N, Dranca I. Variation in activation energy of the glass transition for polymers of different dynamic fragility. Macromolecular Chemistry and Physics 2006;207:1126−30.
[22] Elder JP. Multiple reaction scheme modeling 3: mutually independent nth order reactions. Journal of Thermal Analysis 1989;35:1965−84.
[23] Vyazovkin SV, Lesnikovich AI. On the dependence of kinetic parameters and functions in non-isothermal kinetics. Thermochimica Acta 1987;122:413−8.
[24] Vyazovkin SV, Lesnikovich AI. An approach to the solution of the inverse kinetic problem in the case of complex processes. 1. Methods employing a series of thermoanalytical curves. Thermochimica Acta 1990;165:273−80.